Mon. Not. R. astr. Soc. (1990) **242,** 560–569

Massive thin accretion discs – II. Polarization

Ari Laor and Hagai Netzer
School of Physics and Astronomy and The Wise Observatory, Tel-Aviv University, Tel-Aviv 69978, Israel*

Tsvi Piran
Racah Institute for Physics, The Hebrew University, Jerusalem 91904, Israel

Accepted 1989 August 8. Received 1989 June 14

SUMMARY

Thin accretion discs around massive black holes are believed to produce much of the observed optical-UV emission from AGN. Classical calculations predict that this radiation is highly polarized at large inclination angles, in contrast to observations of quasars and Seyfert galaxies. We have calculated the spectrum and polarization of such discs using an improved radiative transfer method with all the relevant opacity sources, and a full general relativistic treatment of the radiation propagation. We find the overall polarization to be much smaller than previously suggested. At low frequencies the disc opacity significantly reduces its polarization while at high frequencies general relativistic effects depolarize the radiation. The calculated degree of polarization, and its wavelength dependence, are consistent with the available observations. We predict that the degree of polarization should show a distinct broad feature near the Lyman edge, and that the polarization plane should rotate at high frequencies. The first effect will confirm the thermal nature of the observed UV radiation and the second the existence of massive black holes at the centre of AGN.

1 INTRODUCTION

Matter accretion on to massive black holes has been suggested as the main source of energy in the Active Galactic Nuclei (AGN). This may lead to the formation of a thin accretion disc (e.g. Rees 1984) which radiates at optical and UV frequencies (Shields 1978; Malkan & Sargent 1982). There have been several attempts to fit the observed AGN continuum by theoretical disc spectra (Malkan 1983; Czerny & Elvis 1987; Wandel & Petrosian 1988; Sun & Malkan 1987) but the theory of such systems is not yet at the stage that the calculations can be fully trusted and used to deduce the disc parameters, such as the mass, accretion rate and inclination angle. It might even be intrinsically impossible to get any strong bound on these parameters with this method (Laor 1989). Alternative methods for discovering discs must therefore be investigated, in particular those depending on the special geometry (e.g. Netzer 1985). One possibility is to look for the polarization of the disc radiation which is expected to be very large for edge-on systems. The observed polarization is, however, of the order of 1 per cent only (Stockman, Moore & Angel 1984) and there have been attempts to explain this by invoking small-scale structural changes (Coleman & Shields 1989), or by thick accretion tori (Webb & Malkan 1986). These works did not take into account the effects of opacity on the intrinsic polarization, or relativistic effects on the propagation of polarization. Connors & Stark (1977) and Stark & Connors (1977) suggested that relativistic effects can be recognized since they result in a unique, wavelength dependence of the disc-polarized radiation.

In Paper I of this series (Laor & Netzer 1989) we have described new calculations for accretion discs around massive black holes and their application to AGN theory. In the present paper we extend the calculations to include also the polarization of the disc radiation and discuss possible ways of detecting this radiation. We include all the general relativistic effects that are affecting the propagation of light emitted by the disc, and pay special attention to the treatment of opacity, which determines the degree of polarization. This paper follows the work of Connors, Piran & Stark (1980, hereafter CPS), who consider polarization in discs around stellar mass black holes. There are, however, several important differences, mainly in the treatment of opacity, since we are interested in discs around massive black holes, which are much cooler than discs around stellar mass black holes.

In Section 2 we review the theory of polarization and propagation of radiation in Kerr metric in a detailed way to allow the use of the method by others. In Section 3 we demonstrate the relativistic effects by considering a simple, blackbody disc and in Section 4 we explain the calculations

* Of the Raymond and Beverly Sackler Faculty of Exact Sciences.

for AGN-type discs. The results are given in Section 5 and discussed in Section 6. Appendix A gives a short version of the transfer function needed for the relativistic calculations.

2 POLARIZATION CALCULATIONS FOR A THIN KERR DISC

We review in Section 2.1 the propagation of the polarization vector along null geodesics in the Kerr metric. In this presentation we follow the formalism used by CPS. In Section 2.2 we describe the calculation of the transfer functions that relate the intensity and polarization at the disc and the observed spectrum and polarization at infinity. Readers who are not interested in the technical part of the computations can skip both sections.

2.1 Propagation of the polarization vector in the Kerr metric

We describe the polarization of a beam of radiation by the normalized Stokes parameters (Chandrasekhar 1960)

$$X_S = Q/I \quad Y_S = U/I, \tag{1}$$

where I is the intensity and Q, U are the Stokes parameters for determining the linear polarization which results from electron scattering in the disc photosphere. X_S and Y_S range between -1 and $+1$ and they are defined relative to a chosen two-axis, e_1, e_2, such that e_1, e_2 are space-like and orthogonal to the wavevector k. The degree of polarization, δ, and the angle of the plane of polarization, ψ, are given by

$$\delta = \sqrt{X_S^2 + Y_S^2} \quad \psi = \tfrac{1}{2}\tan^{-1}(Y_S/X_S). \tag{2}$$

The direction of polarization of a beam of radiation is described by a unit four-vector, f^μ, which is orthogonal to the wave vector $\mathbf{k}^\mu$. f^μ is parallelly transported along the photons' null geodesic, i.e.

$$\mathbf{k}^\mu \nabla_\mu f^\nu = 0 \quad \mathbf{k}^\mu f_\mu = 0, \tag{3}$$

where ∇_μ is the covariant derivative along the null ray. The degree of polarization is a scalar invariant.

The spacetime around a stationary black hole is described by the Kerr metric (Kerr 1963). We shall use the Boyer–Lindquist coordinates (t, r, θ, ϕ) with geometrical units $(c = G = 1)$. r is measured in gravitational radii of the black hole whose mass is M. A null geodesic in the Kerr metric is described by two constants of motion: L/E and Q/E^2 (where E and L are the energy and angular momentum as measured by an observer at infinity, and Q is Carter's constant of motion). Walker & Penrose (1970) have discovered another complex constant, κ_{pw}, which is conserved along null geodesics in the Kerr metric. Connors & Stark (1977) have pointed out that this constant describes the parallel transport of the polarization vector, f^μ along the null geodesic. We normalize $\mathbf{k}^\mu$ such that $\mathbf{k}_0 = -1$ and then we define

$$\begin{aligned}\kappa_{pw} = \kappa_2 - i\kappa_1 = \{&(\mathbf{k}^t f^r - \mathbf{k}^r f^t) + a\sin^2\theta(\mathbf{k}^r f^\phi - \mathbf{k}^\phi f^r) \\ &- i[(r^2 + a^2)(\mathbf{k}^\phi f^\theta - f^\phi \mathbf{k}^\theta) - a(\mathbf{k}^t f^\theta \\ &- \mathbf{k}^\theta f^t)]\sin\theta\}(r - ia\cos\theta).\end{aligned} \tag{4}$$

Following CPS we express the three space-like components of f^μ for an observer at θ_0 at infinity in terms of the constants of motion

$$\begin{aligned} f_r = 0 \quad f_\theta &= (S\kappa_1 - T\kappa_2)/(S^2 + T^2) \\ f_\phi &= (-S\kappa_2 - T\kappa_1)/(S^2 + T^2), \end{aligned} \tag{5}$$

where $S = (L/E\sin\theta_0 - a\sin\theta_0)$, $T = \mathrm{sgn}(\kappa^\theta)_\infty[Q/E^2 - (L^2/E^2)\cot^2\theta_0 + a^2\cos^2\theta_0]^{1/2}$ and f_θ, f_ϕ are defined relative to the fixed 2-axis e_θ, e_ϕ at infinity for an observer at polar angle θ_0.

2.2 The transfer functions

To obtain the spectrum at infinity we define a transfer function T which transforms the local spectrum of the disc to that seen by an observer at infinity. We denote by subscript 'e' all quantities at the rest frame of the emission radius r_e, and by a subscript 'o' quantities for an observer at infinity at polar angle θ_0. For a given geometrically thin disc model the locally emitted intensity, I_e, is a function of ν_e, r_e and θ_e, the angle between the normal to the disc and the direction in which the ray leaves the disc. We define the transfer function, T, by the relation between the observed flux and emitted intensity

$$\begin{aligned} F_0(\theta_0, \nu_0) &= \int r_e\, dr_e\, d\phi_e\, d\cos\theta_e\, dg I_e(r_e, \nu_0/g) L(\theta_e)\,\delta \\ &\quad \times [\theta_0 - \theta_e(r_e, \theta_e, \phi_e)]\,\delta[\nu_e - \nu_0/g(r_e, \theta_e, \phi_e)] \\ &\equiv \int dg r_e\, dr_e\, T(\theta_0, r_e, g) I_e(r_e, \nu_0/g), \end{aligned} \tag{6}$$

where $g = \nu_0/\nu_e = (1+z)^{-1}$ (and z is the photon's redshift). The most general transfer function will depend on θ_e as well. In writing equation (6), we have assumed a specific, frequency-independent, limb-darkening law $I_e(r_e, \nu_e, \theta_e) = I_e(r_e, \nu_e)L(\theta_e)$. This allows us to integrate over θ_e and to eliminate one variable from T. Clearly with this choice our transfer function is limited for the specific $L(\theta_e)$ that we have chosen (see equation 12).

The transfer function T transfers the emitted spectrum at the disc to the observed flux at infinity. To calculate the polarization we define two additional transfer functions T_X and T_Y that transfer the components of the polarization. $T_X(\theta_0, r_e, g)$ relates the flux of radiation in the ϕ plane at θ_0 and at frequency $\nu_0 = \nu_e g$ at infinity to the intensity of the radiation at r_e and at frequency ν_e. T_Y is the transfer function for the orthogonal polarization.

In order to calculate these general relativistic radiation transfer functions we use the following numerical procedure. At each radius we 'emit' a given number of photons isotropically (at the local frame of the matter). Each photon has a local energy $\tilde{\mathbf{k}}^0 = 1$ relative to the local rest frame of the matter and it has a statistical weight, s_i, corresponding to the limb-darkening law $L(\theta_e)$ so that the integrated weight of all photons is unity. The initial polarization angle is taken as parallel to the disc surface, and the initial polarization intensity, δ_i, is given by the Chandrasekhar (1960) formulae for polarization of optically thick discs. A calculation of the photon's energy relative to infinity, yields immediately the energy shift factor since (with $\tilde{\mathbf{k}}^0 = 1$) $g = E$. We integrate the geodesic equation and obtain θ_0 and f^θ and f^ϕ, which define the polarization plane at infinity. The overall transfer function for the intensity is

$$T(\theta_0, r_e g) = \Sigma s_i, \tag{7}$$

where the summation is over all photons emitted at r_e which reach $\theta_0 \pm d\theta_0/2$ with $g \pm dg/2$. To obtain the polarization transfer functions we use $\psi = \cos^{-1} f^{\theta}$ and

$$T_X = \Sigma s_i \delta_i \cos 2\psi \quad T_Y = \Sigma s_i \delta_i \sin 2\psi, \tag{8}$$

where the summation is over the same photons.

In our calculations for a rotating black hole $d \ln g = 0.1027 (0.1 \leq g \leq 1.7)$, $d \ln (\cos \theta_0) = 0.0826$ and we have used 35 different values of $r_e (r_e = 1600/N^2, 2 \leq N \leq 36)$, with 10 000 photons per radius. With these parameters T has converged to better than 1 per cent. This calculation was done also for a non-rotating black hole. The accuracy of the code used for calculating the trajectory was verified by comparison with the published results of Cunningham (1975) and CPS. This numerical method is more efficient than the one applied by Cunningham (1975), if one wishes to calculate T for all angles simultaneously. We start from a given r_e and calculate every trajectory to infinity only once, whereas in Cunningham's method one starts at infinity from a given θ_0 and finds, by iterations, the trajectories which started from a given r_e. Our results and those of Cunningham (1975) are somewhat different, and the reason is explained below.

A small fraction of all the photons is captured by the black hole (Thorne 1974), which results in a small reduction in the observed flux. A larger part returns to the disc (Cunningham 1976). We assumed that these photons are absorbed and re-emitted after being thermalized locally. Cunningham (1975) ignores this effect. This results in an increase in the effective temperature, especially near the inner edge of the disc. This correction for the locally emitted flux was taken into account by solving the equation

$$F_e(r) = F_g(r) + \int T_a(r, r_e) F_e(r_e) r_e r^{-1} \, dr_e, \tag{9}$$

where $F_g(r)$ is the flux generated locally per unit area at r, $F_e(r)$ is the emitted flux and $T_a(r, r_e)$ is another transfer function that gives the fraction of the flux absorbed per unit area at r from a unit area at r_e. This transfer function depends on the angular distribution of the emitted flux, but not on its absolute value, and it was calculated during the calculation of the transfer function that was discussed before. When a photon emitted at r_e intersects the disc at r it contributes to $T_a(r, r_e)$.

$$T_a(r, r_e) = \sum s_i \frac{E_i}{\bar{E}(r)}, \tag{10}$$

where $\bar{E}(r)$ is the average energy of photons observed at infinity from r. In the case of a rotating black hole the correction is approximately 20 per cent over most of the disc, with a sharp rise at the inner edge. The rise is not observationally significant as most of the radiation from the inner edge is trapped by the black hole. Both these absorption effects are insignificant in a non-rotating black hole.

A short version of the transfer function is tabulated in Appendix A and the full tabulation is available from the authors upon request.

3 GENERAL RELATIVISTIC RESULTS FOR A BLACKBODY DISC

General relativistic effects depolarize the intrinsic disc radiation in two different ways. First, the radiation observed at a given angle relative to the disc axis is emitted, in most cases, at a smaller angle and is bent towards the plane of the disc. The resulting polarization is, therefore, lower than expected at such angles. Secondly, the plane of polarization is rotated by an amount which depends on the radius of emission. The spectrum, at a given frequency, has contributions from a range of radii with various rotations, and their sum has a lower degree of polarization. Apart from these effects the disc's intrinsic polarization can be strongly modified by the opacity in its atmosphere.

In this section we illustrate the relativistic effects by considering a simple case where the local opacity plays no role in the calculation. In Section 4 we combine this with the treatment of a more realistic disc atmosphere. To demonstrate the general relativistic effects we consider first a simple case of a blackbody disc with a fully scattering atmosphere (no absorption). The disc structure was calculated using the general relativistic equations of Novikov & Thorne (1973) and Page & Thorne (1974) as described in Paper I. The local intensity was taken to be a Planck function with the local effective temperature, and does not depend on the density, pressure and vertical temperature gradient. The outer edge of the disc was taken as the self-gravity radius (Paper I). This radius depends on the assumed parameters of the model (see next section) and affects the spectrum at the low-frequency end, where the general relativistic effects are negligible. The local degree and plane of polarization are taken from Chandrasekhar (1960).

Results for the spectrum, degree and plane of polarization are shown in Figs 1 and 2, for cases of a non-rotating black hole and the canonical rotating black hole inside a disc ($a/M = 0.9982$, Thorne 1974). The basic parameters are the accretion rate, $\dot{m}$, measured in units of the Eddington accretion rate, the mass of the black hole, m_9, measured in units of $10^9 M_\odot$, and the disc inclination angle, θ_0 ($\mu = \cos \theta_0$). We show the results for three angles: nearly face on ($\mu = 0.96$), average inclination ($\mu = 0.5$) and close to edge on ($\mu = 0.1$). (The assumption that the emitting surface is at right angles to the disc axis is not strictly correct at small r_e, especially for high accretion rates. This can introduce significant errors for very small μ.) The spectrum of a disc around a rotating black hole, shown in Fig. 2, is somewhat different from the one given by Cunningham (1975). This is because we include a correction due to re-absorption of the emitted flux, which was neglected by Cunningham. This is not a negligible effect since the disc absorbs and re-emits about 17 per cent of the total flux as observed at infinity.

The general relativistic effects are very noticeable and result in a decreasing polarization at high frequencies compared with the classical, frequency-independent, polarization. The effects are much larger for a rotating black hole where the disc extends to regions much closer to the black hole, and are most noticeable at the high-frequency part of the spectrum, which is emitted by the inner hot part of the disc. The degree of polarization varies with frequency (Figs 1b and 2b) because of the two processes described below.

(i) The first is the change in the direction of the photon due to general relativistic bending and special relativistic beaming. This is most noticeable at large θ_0. The higher frequency photons are emitted at smaller r_e and smaller θ_e and are less polarized, thus the overall polarization decreases

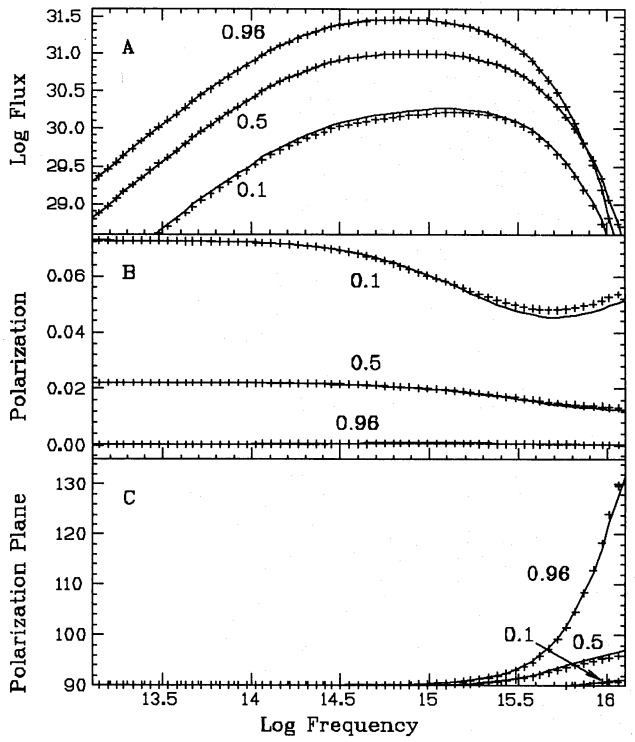

Figure 1. Spectrum and polarization of a blackbody disc around a nonrotating black hole with $m_9 = 1$ and $\dot{m} = 0.3$. The disc inclination (μ) is marked on the curves. Solid line: transfer function for a nonrotating black hole. + +: transfer function of a rotating black hole. The results can be scaled to any mass or accretion rate by multiplying the frequency by $m_9^{-1/4}(\dot{m}/0.3)^{1/4}$. (A) Observed flux. Units here, and in all following diagrams, are: erg s^{-1} cm^{-2} Hz^{-1} (for different m_9 and $\dot{m}$ the flux should be multiplied by $m_9^{5/4}(\dot{m}/0.3)^{3/4}$). (B) The observed degree of polarization. (C) The observed angle of the polarization plane. 90 degrees is parallel to the disc plane (i.e. no rotation).

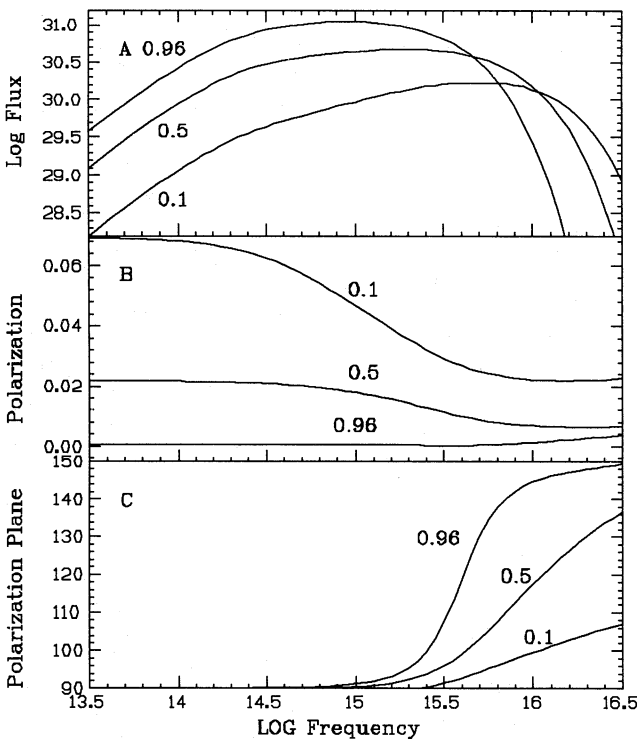

Figure 2. Same as in Fig. 1 for a rotating black hole.

with frequency. At small θ_0 the higher frequency photons, that are emitted at smaller r_e, have higher θ_e and higher polarization, so the overall degree of polarization increases. In absolute terms, depolarization at high inclinations is much greater than repolarization at low inclinations, as is evident from Fig. 2(b).

(ii) The second is the rotation of the plane of polarization. This causes depolarization by combining photons of different polarization angles. It is significant only at very small r_e, i.e. at the very high-frequency part of the spectrum. The effect is most noticeable at small θ_0.

The angle of the plane of polarization, ψ, is shown in Figs 1(c) and 2(c). $\psi = 90°$ is the Newtonian case of polarization plane parallel to the disc surface. The rotation of ψ is larger at low inclination angles where the degree of polarization is smaller. For a non-rotating black hole this rotation is significant only at high frequencies, where the emitted flux is very small. In the rotating black hole case the effect is strong at lower frequencies, where the emitted flux is significant.

Similar general relativistic results, for a $9M_\odot$ black hole accreting at about $\dot{m} = 0.2$, are shown in CPS. Their results are somewhat different from ours because they used a modified blackbody spectrum (Novikov & Thorne 1973). This gives a more effective depolarization in their model, since a larger region in the disc contributes significantly at a given frequency. A further and obvious difference is the overall frequency range; optical-UV in this paper (very massive black hole) versus soft to hard X-rays in CPS (stellar size black hole).

The results shown in Figs 1 and 2 can be scaled to any mass or accretion rate by multiplying the frequency by $m_9^{-1/4}(\dot{m}/0.3)^{1/4}$, and the flux by $m_9^{5/4}(\dot{m}/0.3)^{3/4}$. Note that the results given by CPS should not be scaled in a similar manner since they used the modified blackbody approximation, which is not appropriate for a disc around a massive black hole. There is an additional and small correction at the low-frequency end due to the dependence of the self-gravity radius on m_9 and $\dot{m}$. All the relativistic effects are insignificant at such low frequencies.

Finally, we show in Fig. 1 a comparison of the transfer functions for rotating and non-rotating black holes by repeating the calculations for a non-rotating black hole using the rotating black hole transfer function. It is evident from the diagram that the difference between the two is very small, and the transfer function used for the rotating black hole can be applied also in the non-rotating case (obviously the two are similar only for $r \geq 6$, which is outside the inner radius of the disc in the non-rotating black hole case). In Appendix A we list only the transfer function for a rotating black hole.

4 REALISTIC DISC MODELS

The general relativistic effects described in the previous section have been combined with more realistic disc models (Paper I) to investigate the disc spectrum and polarization. Before describing our results a general comment about the present status of disc models is in order. We do not attempt

to give a self-consistent solution for the vertical structure of the disc and its atmosphere. To the best of our knowledge such models are not yet available, partly because of their complexity and mainly because they depend, critically, on the poorly understood viscosity mechanism. Our model includes full general relativistic treatment of the disc structure and spectrum. Our radiative transfer method, though not a proper atmosphere solution, takes into account realistic opacities and the effect of the vertical temperature gradient. Other recently published calculations for such discs used the local blackbody approximation (e.g. Sun & Malkan 1987), assumed a modified blackbody without general-relativistic effects (Czerny & Elvis 1987; Wandel & Petrosian 1988), or combined published stellar atmospheres (Sun & Malkan 1987). A recently published paper by Litchfield, King & Brooker (1989) also combines stellar atmospheres, but it does not include any general relativistic effects.

4.1 Disc structure and local spectrum

The structure and spectrum of thin accretion discs have been calculated in Paper I. Here we review only the main features of the model and refer the reader to Paper I for more details.

We calculated the structure and the spectrum of thin accretion discs around massive black holes. The radial and vertical structure were calculated using the α disc approximation (Shakura & Sunyaev 1973) with the general relativistic corrections as given by Novikov & Thorne (1973) and Page & Thorne (1974). We considered three viscosity laws: (*1*) $t_{r\phi}=\alpha(P_g+P_r)$, (*2*) $t_{r\phi}=\alpha P_g$ and (*3*) $t_{r\phi}=\alpha\sqrt{P_gP_r}$, where $t_{r\phi}$ is the viscous stress, P_g is the gas pressure and P_r is the radiation pressure. A self-consistent thin disc model requires that $\dot{m}\leq 0.3$ and $\alpha\leq 0.1$ (Paper I). We have calculated the local spectrum using the Eddington approximation for an atmosphere dominated by electron scattering, with a vertical temperature gradient. This is an improvement compared with some earlier calculations where a local blackbody or modified blackbody was assumed, but is still far from a full atmospheric solution, as required. For example we found the surface temperature to be close to the effective temperature, even when electron scattering strongly dominates the opacity, while earlier studies (e.g. Czerny & Elvis 1987) found a significantly higher surface temperature.

For the opacity calculations we considered hydrogen and helium bound–free transitions for $n\leq 4$, free–free absorption and electron scattering. These are the main opacity sources for the temperatures ($10^4<T<10^5$ K) and frequencies ($3\times10^{14}<\nu<10^{16}$) that are typical of accretion discs around massive black holes. The bound–free contribution to the opacity is significant, and results in a wavelength-dependent absorption. Previous studies of this problem (e.g. Shakura & Sunyaev 1973) assumed free–free absorption only, or increased the free–free absorption to compensate for the bound–free opacity (Czerny & Elvis 1987; Wandel & Petrosian 1988). The second approximation resulted in a wrong wavelength dependence for the opacity with important implications for the observed polarization (Section 5).

The absorption opacity depends strongly on temperature, regardless of density, and all models share the obvious trend of a decrease in the absorption opacity at smaller radii. The absorption opacity is also proportional to the density, and it thus depends on the viscosity law used (Paper I). This must be kept in mind when calculating the polarization, as is shown below.

4.2 Intrinsic polarization

Electron scattering was taken as the only source of polarization (Chandrasekhar 1960). The local degree of polarization depends on the relative importance of the different sources of opacity. We define a weighing factor $q(\nu)$ by

$$q(\nu)=\frac{\kappa_{es}}{\kappa_{es}+\kappa_{ab}(\nu)}, \tag{11}$$

where κ_{es} is the electron scattering opacity and $\kappa_{ab}(\nu)$ is the absorption opacity. This factor multiplies the classical Chandrasekhar expression for the polarization. Generally speaking, models with higher density have smaller q(ν) and lower polarization. The strong temperature dependence of $\kappa_{ab}(\nu)$ causes $q(\nu)$ to increases with frequency in all models. The contribution of bound–free absorption is not continuous and $q(\nu)$ can have large discontinuous drops at frequencies just above absorption edges.

Gnedin & Silant'ev (1978) have calculated the polarization from an atmosphere with a source function which varies linearly with τ, and $q(\nu)$ which is independent of τ. The intrinsic polarization that they found is somewhat different from ours. In particular, they found that when the source function gradient in the atmosphere is very small, the plane of polarization rotates by 90 degrees. The rotation occurs because in a nearly isothermal atmosphere most photons are moving in parallel to the disc surface before the last scattering event, thus the polarization is orthogonal to the disc surface. Cheng *et al.* (1988) have shown that this effect occurs only at low frequencies, where the degree of polarization is very low ($\leq$0.1 per cent). We therefore neglected this effect entirely.

Sunyaev & Titarchuk (1985) and Phillip & Mészáros (1986) showed that the polarization can differ significantly from the classical Chandrasekhar results when the optical depth for electron scattering is approximately unity. Such small optical depths do not occur in our models and the local polarization should not deviate significantly from Chandrasekhar's law scaled by our $q(\nu)$.

4.3 Limb darkening

We assumed a linear limb-darkening law of the form

$$\frac{L(\mu)}{L(1)}=\frac{1+a\mu}{1+a}. \tag{12}$$

In an optically thick electron scattering atmosphere, $a=2.06$ (e.g. Phillip & Mészáros 1986), whereas in a non-scattering grey atmosphere, $a=1.5$. A general, full radiative transfer calculation can be significantly more complicated. It produces a non-linear limb-darkening law (see Wade & Rucinski 1985) which depends on the effective temperature, gravity and composition of the atmosphere and is also a function of frequency. We have chosen a model and frequency-independent limb-darkening law, with $a=2.06$, in order to simplify our calculation. This should approximate well the region of the disc dominated by electron scattering,

as was verified by comparison with the relevant models published by Wade & Rucinski (1985). It allowed us to greatly simplify the transfer function, as explained in the previous section.

The last step in the calculations involves the combination of the local spectrum and polarization with the transfer function (Section 3) to obtain the spectrum and polarization as observed at infinity.

5 RESULTS

Figs 3 and 4 show the degree and plane of polarization for a rotating black hole for several combinations of m_9, $\dot{m}$, α, μ and viscosity laws. All the models share the following properties.

(i) A low degree of polarization over the range $14 \leq \log(\nu) \leq 14.5$. This radiation comes from the relatively cold parts of the disc where $q(\nu)$ is small.

(ii) A continuous increase in the degree of polarization over the range $14.5 \leq \log(\nu) \leq 15.5$ due to decreasing absorption opacity at high frequencies. The amplitude of this increase depends mainly on the disc inclination and to some extent on the other model parameters which determine the value of $q(\nu)$.

(iii) A very broad feature around $\log(\nu) = 15.5$, due to the Lyman edge in absorption and the corresponding drop in polarization. The absorption above that edge decreases monotonically and the polarization increases. This feature is broadened significantly by the various Doppler shifts and by the gradient in the gravitational redshift. In colder discs the region of interest is closer to the black hole, and the peak of the feature occurs at lower frequencies and is broader. This can be seen in Fig. 3 in which we compare the polarization from a 'hot' disc ($m_9 = 0.01$) with the polarization from a cooler disc ($m_9 = 1.0$).

(iv) For $\log(\nu) \geq 16$ the absorption is negligible in most models and the degree of polarization approaches the general relativistic limit (Section 3). In viscosity law (*2*) the density is the highest and the absorption is most significant. This is the only case where we observe a significant feature due to the He^+ bound–free absorption edge.

(v) The rotation of the plane of polarization, for a given inclination, resembles the blackbody disc results (Section 3) in all the models. The opacity modifies only the degree of polarization, not its orientation. The small variations relative to the blackbody case are due to the differences in surface temperature.

Results for the non-rotating black hole case are shown in Fig. 5. Although the general properties are similar to the rotating black hole case, the general relativistic effects are very small and the degree of polarization is determined mainly by the opacity. Considerable rotation of the plane of polarization occurs only at frequencies well above the maximum flux frequency.

6 DISCUSSION

Our calculations demonstrate that the commonly accepted view (e.g. Antonucci 1988) that thin accretion discs in AGN

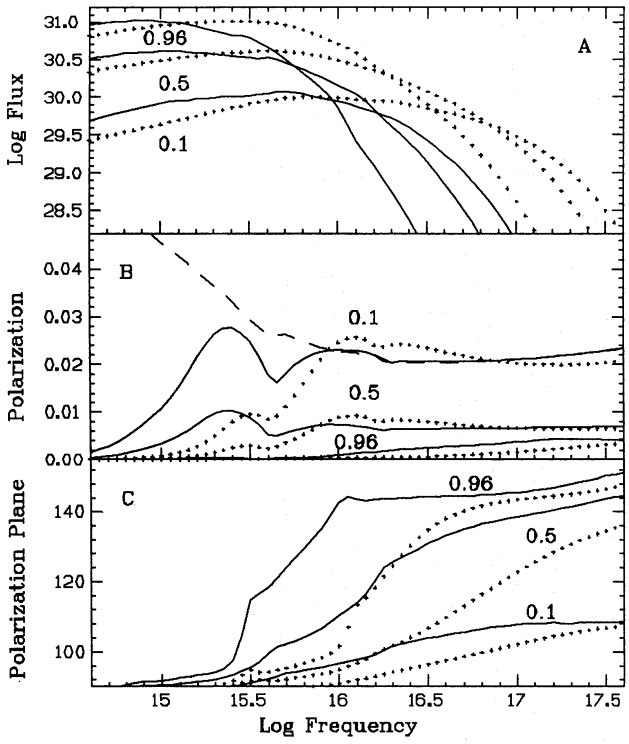

Figure 3. Spectrum and polarization for model discs. Here $\alpha = 0.1$, the viscosity law is *1*, a rotating black hole with $\dot{m} = 0.3$. Solid line: $m_9 = 1$. Dotted line: $m_9 = 0.01$. (A) Observed flux (the dotted line is shifted vertically by +2.5). (B) The observed degree of polarization. Note the broad feature at $\nu \sim 10^{15.5}$. Dashed line: the degree of polarization with no opacity effects for $\mu = 0.1$. (C) The observed angle of the polarization plane.

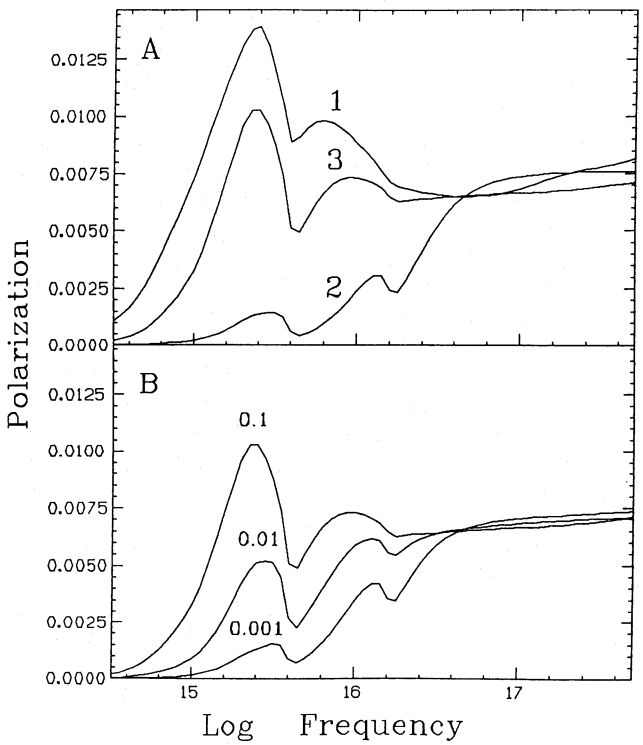

Figure 4. Degree of polarization for various model parameters, for a disc around a rotating black hole with $m_9 = 1$, $\dot{m} = 0.3$ and $\mu = 0.5$. (A) Different viscosity laws as marked on the curves (see text), all with $\alpha = 0.1$. (B) Viscosity law *3* and different α, as marked.

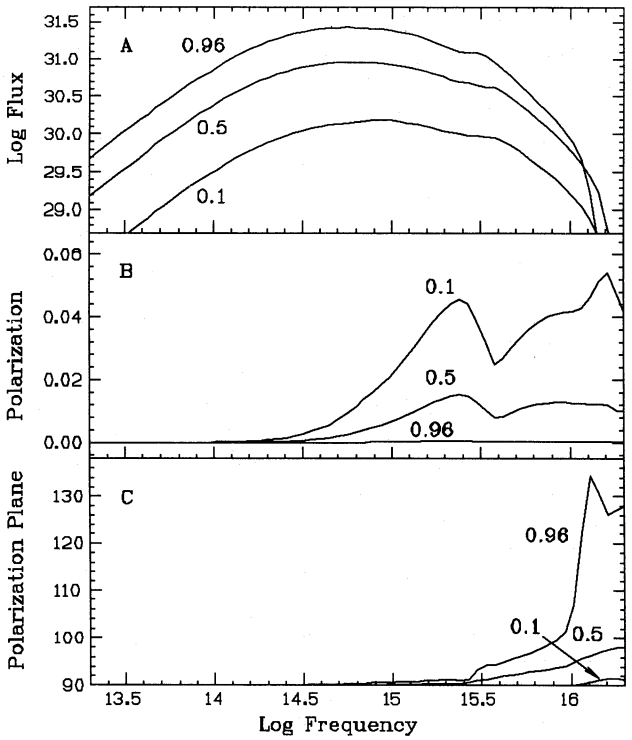

Figure 5. Same as in Fig. 3 for a non-rotating black hole.

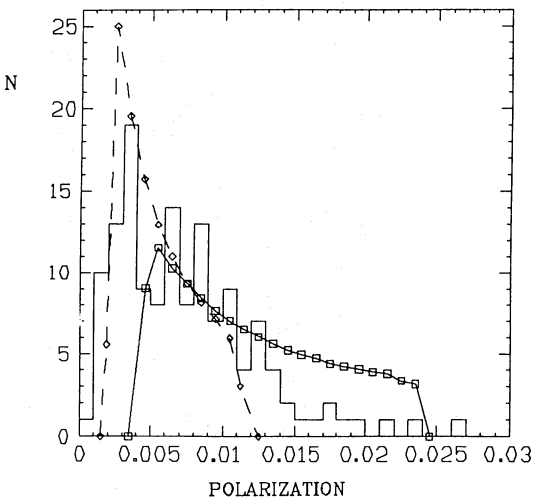

Figure 6. The distribution of the number of quasars as a function of the degree of polarization. The results of the two models of a rotating black hole with $\dot{m}=0.3$ and viscosity case *1* are compared with the observations of Stockman *et al.* Solid line: $m_9=1$. Dashed line $m_9=0.1$.

can be recognized by their large degree of polarization is not realistic. In the high-frequency range general relativistic effects depolarize the radiation, while at low to intermediate frequencies the polarization is reduced by the absorption opacity. Thus one does not have to introduce any irregularities in the disc surface, as suggested by Coleman & Shields (1989), in order to explain the low observed polarization. The general relativistic depolarization is small for a non-rotating black hole, but such a black hole is not very physical as it will be spun up on a cosmologically short time-scale (Page & Thorne 1974). Depolarization due to opacity is model dependent, but all models, including those with relatively low density, show this effect to be significant. For example, the regions in the disc that dominate the flux emission at $\nu \sim 5\times10^{14}$ Hz ($T_{\rm eff}\sim10^4$ K) have $q(\nu)\ll1$, unless the density is extremely low.

Cheng *et al.* (1988) used published stellar atmosphere models to calculate the degree of polarization of thermal radiation from accretion discs around dwarf novae, where the relativistic effects are negligible. They found that the polarization is significantly reduced, compared with the classical atmosphere, even for effective temperatures as high as 50 000 K. They also found a sharp drop in polarization above the Balmer edge, similar to the one we find beyond the Lyman edge. Their results relating the disc opacity and polarization support ours, although one should remember that it is still not clear how realistic the stellar atmosphere approximation for the disc is.

Stockman, Moore & Angel (1984) studied the optical polarization properties of low-polarization quasars which constitute more than 90 per cent of all quasars. They found that the white light polarization ranges typically between 0 and 2 per cent, with an average of 0.6 per cent. In Fig. 6 we compare the observed distribution of the number of quasars as a function of polarization at $\nu=10^{15}$ Hz (this represents the optical region for a redshift of 0.7, which is typical for that sample) with the one we calculated assuming a random distribution of disc orientations with two different black hole masses. The agreement is encouraging, but one should note that it was obtained for viscosity law (*1*) and $m_9=1$ and 0.1. These parameters give a degree of polarization in the optical region, which is somewhat higher than for other parameters. The sample of quasars is not well defined and it is not clear how its selection affects the results. Furthermore, other components in the spectrum probably influence the observed polarization. Stockman *et al.* also list the degrees of polarization for a subsample of 15 quasars that were observed in two colours. Fig. 7 shows their data (plotted at rest frequency) and compares them with theoretical results for various disc inclinations in a specific disc model. The observed increase in polarization with frequency is similar to that predicted by the theoretical calculations. Note that a model with a relatively high degree of polarization was used, which is consistent with the fact that these objects have a higher than average degree of polarization. Further spectropolarimetric observations with higher spectral resolution are needed in order to test our model. Stockman, Angel & Miley (1979) found the polarization to be generally parallel to the observed radio axis; this might be in conflict with the polarization plane expected in thin discs, if one assumes this axis to be parallel to the disc axis. Finally, Stockman *et al.* find no change in the angle of polarization, in agreement with our theoretical results which show significant rotation of the polarization plane only at frequencies well above 10^{15} Hz.

In high polarization quasars the polarization is significant at near infrared frequencies (e.g. Smith *et al.* 1987), and it can decrease at shorter wavelengths (Wills 1989). Such a polarization cannot be due to thermal emission from an accretion disc. It must result from a different mechanism, most probably a non-thermal process.

The Lyman edge absorption has been suggested by Antonucci, Kinney & Ford (1989) as a test of the idea that

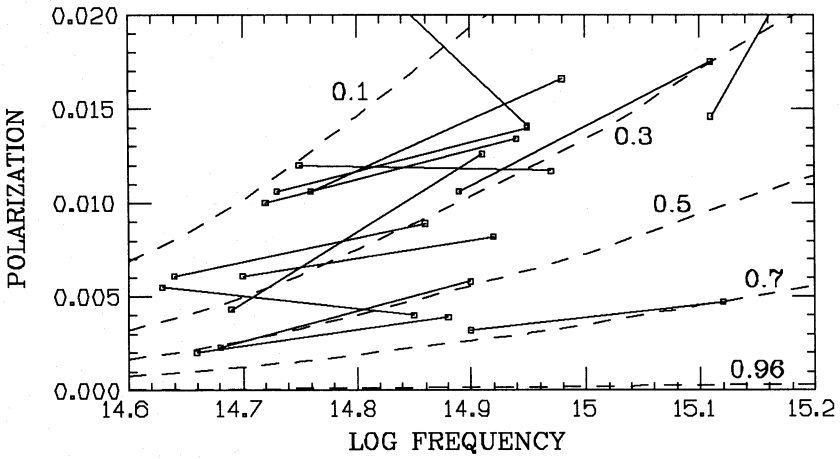

Figure 7. Degree of polarization as a function of rest frequency. The objects shown are from the sample of Stockman *et al.* Each object is represented by a line connecting the measurements in the *B* and *R* broadband filters. The error bars, typically 0.3 per cent, are not drawn for the sake of clarity. The model is for a disc around a non-rotating black hole with $m_9 = 1$, $\dot{m} = 0.3$, $\alpha = 0.1$ and viscosity law *l*. The inclination angle is marked on the curves.

the UV bump in AGN is emitted by an accretion disc. This suggestion is based on the fact that stellar spectra generally show strong absorption beyond the Lyman edge. Yet model stellar atmospheres with very high effective temperature, similar to the temperatures in AGN accretion discs, generally show a much smaller absorption edge (e.g. Kurucz 1979). An emission jump (for H_e^+) may appear when non-LTE effects are fully taken into account (Husfeld *et al.* 1984). Thus direct observations of the Lyman limit absorption edge may not be a good test for accretion discs.

Our model suggests a different, perhaps more reliable and less model-dependent test for such discs, based on the significant drop in polarization beyond the Lyman edge. A broad feature due to the change in opacity appears in all models, regardless of the strength of the Lyman jump. This feature is very broad due to relativistic effects (Figs 3–5) and care must be taken in observing it since the frequency range of interest can be dominated by Lyman line absorption systems in the spectrum of high-redshift quasars. Such absorption systems make the observation more difficult and can change the quasars' intrinsic polarization in an unknown way.

A further prediction of the model is the rotation of the plane of polarization. Unlike the degree of polarization, this does not depend on the viscosity law used, only on m_9 and $\dot{m}$. As already suggested by CPS for a solar mass black hole, the discovery of such a rotation will be the first direct indication for the existence of a very massive black hole at the quasar's core. If the amount of rotation conforms to our theoretical calculation, it will further indicate that the matter which emits this radiation is indeed orbiting in a thin accretion disc. Unfortunately, the rotation is largest for face-on discs, where the polarization is the smallest and it is significant only at very high frequencies ($\geq 10^{16}$ Hz). A search for such a rotation requires high-resolution UV spectropolarimetry of high-redshift quasars, a feasible, yet a very difficult task for the Hubble Space Telescope.

ACKNOWLEDGMENTS

AL and HN thank B. and D. Wills for helpful discussions. This work was supported by grant No. 85/00085 from the United States–Israel Binational Science Foundation (BSF), Jerusalem, Israel. TP thanks the School of Physics and Astronomy at Tel-Aviv University for hospitality while the research was carried out. The research was also partially supported by a BSF grant to the Hebrew University.

REFERENCES

Antonucci, R., 1988. In: *Supermassive Black Holes*, p. 26, ed. Kafatos, M., Cambridge University Press, Cambridge.
Antonucci, R., Kinney, A. & Ford, H., 1989. *Astrophys. J.*, **342,** 64.
Chandrasekhar, S., 1960. *Radiative Transfer*, Dover Publications, New York.
Cheng, F. H., Shields, G. A., Lin, D. N. C. & Pringle, J., 1988. *Astrophys. J.*, **328,** 223.
Coleman, H. H. & Shields, G. A., 1989. Preprint.
Connors, P. A. & Stark, R. F., 1977. *Nature*, **269,** 128.
Connors, P. A., Piran, T. & Stark, R. F., 1980. *Astrophys. J.*, **235,** 224 (CPS).
Cunningham, C. T., 1975. *Astrophys. J.*, **202,** 788.
Cunningham, C. T., 1976. *Astrophys. J.*, **208,** 534.
Czerny, B. & Elvis, M., 1987. *Astrophys. J.*, **312,** 325.
Gnedin, Yu. N. & Silant'ev, N. A., 1978. *Soviet Astr.*, **22,** 325.
Husfeld, D., Kudritzki, R. P., Simon, K. P. & Clegg, R. E. S., 1984. *Astr. Astrophys.*, **134,** 139.
Kerr, R. P., 1963. *Phys. Rev. Lett.*, **11,** 237.
Kurucz, R. L., 1979. *Astrophys. J. Suppl*, **40,** 1.
Laor, A., 1989. In: *Active Galactic Nuclei, IAU Symp. No. 134,* p. 25, eds Osterbrock, D. E. & Miller, J. S., Kluwer, Dordrecht.
Laor, A. & Netzer, H., 1989. *Mon. Not. R. astr. Soc.*, **238,** 897.
Litchfield, S. J., King, A. R. & Brooker, J. R. E., 1989. *Mon. Not. R. astr. Soc.*, **237,** 1067.
Malkan, M. A., 1983. *Astrophys. J.*, **268,** 582.
Malkan, M. A. & Sargent, W. L., 1982. *Astrophys. J.*, **254,** 22.
Netzer, H., 1985. *Mon. Not. R. astr. Soc.*, **216,** 63.
Novikov, I. & Thorne, K. S., 1973. In: *Black Holes,* p. 422, eds de Witt, C. & de Witt, B., Gordon & Breach, New York.
Page, D. N. & Thorne, K. S., 1974. *Astrophys. J.*, **191,** 499.
Phillip, K. C. & Mészáros, P., 1986. *Astrophys. J.*, **310,** 284.
Rees, M. J., 1984. *Ann. Rev. Astr. Astrophys.*, **22,** 471.
Shakura, N. I. & Sunyaev, R. A., 1973. *Astr. Astrophys.*, **24,** 337.
Shields, G. A., 1978. *Nature,* **272,** 706.
Smith, P. S., Balonek, T. J., Elston, R. & Heckert, P. A., 1987. *Astrophys. J. Suppl.*, **64,** 459.

Stark, R. F. & Connors, P. A., 1977. *Nature,* **266,** 429.
Stockman, H. S., Angel, J. R. P. & Miley, G. K., 1979. *Astrophys. J.,* **227,** L55.
Stockman, H. S., Moore, R. L. & Angel, J. R. P., 1984. *Astrophys. J.,* **279,** 485.
Sun, W. H. & Malkan, M. A., 1987. In: *Astrophysical Jets and Their Engines,* ed. Kundt, W., Reidel, Dordrecht.
Sunyaev, R. A. & Titarchuk, L. G., 1985. *Astr. Astrophys.,* **143,** 374.
Thorne, K. S., 1974. *Astrophys. J.,* **191,** 507.
Wade, R. A. & Rucinski, S. M., 1985. *Astr. Astrophys. Suppl.,* **60,** 471.
Walker, M. & Penrose, R., 1970. *Commun. Math. Phys.,* **18,** 265.
Wandel, A. & Petrosian, V., 1988. *Astrophys. J.,* **329,** LII.
Webb, W. & Malkan, M., 1986. In: *The Physics of Accretion Onto Compact Objects,* p. 15, eds. Mason, K. O., Watson, M. G. & White, N. E., Springer-Verlag, Berlin.
Wills, B. J., 1989. In: *BL Lac Objects: 10 Years After,* ed. Maraschi, L., Springer-Verlag, Berlin, in press.

APPENDIX A

We show here a short version of the transfer function. The three tables shown represent a disc seen nearly face on ($\mu = 0.96$), close to edge on ($\mu = 0.1$) and at average inclination ($\mu = 0.5$). The first row in each table represents g at the centre of the bin. For each pair of r_e and g we give the elements of the three transfer functions: T, T_X and T_Y. The full transfer function includes 35 bins in r_e, 30 bins in g and 30 bins in θ_0.

Table A1. Elements from the transfer function for $\cos\theta_0 = 0.1$.

r_e/g	0.198	0.266	0.356	0.477	0.640	0.858	1.150	1.542
25.00	0	0	0	0	0	0.695E-01	0.905E-01	0
	0	0	0	0	0	−0.378E-02	−0.559E-02	0
	0	0	0	0	0	0.276E-03	−0.878E-04	0
11.11	0	0	0	0	0.371E-01	0.768E-01	0.116	0
	0	0	0	0	−0.184E-02	−0.182E-02	−0.616E-02	0
	0	0	0	0	0.427E-03	0.429E-03	−0.228E-03	0
6.25	0	0	0	0.101E-01	0.303E-01	0.570E-01	0.176	0.198E-01
	0	0	0	−0.689E-03	−0.455E-03	−0.967E-03	−0.740E-02	−0.118E-02
	0	0	0	0.150E-03	0.204E-03	0.528E-04	−0.582E-03	−0.889E-04
4.00	0	0	0.166E-01	0.860E-02	0.105	0.228	0.239	0.839E-01
	0	0	−0.474E-03	−0.180E-03	0.569E-04	−0.103E-02	−0.639E-02	−0.427E-02
	0	0	0.462E-03	0.638E-04	0.440E-03	0.246E-03	−0.103E-02	−0.599E-03
2.78	0	0.107E-01	0.712E-03	0.223E-01	0.445E-01	0.947E-01	0.265	0.191
	0	−0.186E-03	−0.667E-04	0.508E-04	−0.125E-03	−0.440E-03	−0.389E-02	−0.683E-02
	0	0.297E-03	−0.267E-05	0.927E-05	−0.102E-04	−0.861E-04	−0.136E-02	−0.188E-02
2.04	0.559E-03	0	0.808E-03	0.103E-01	0.620E-02	0.112	0.214	0.324
	−0.567E-04	0	−0.771E-04	−0.969E-04	−0.219E-03	−0.401E-03	−0.180E-02	−0.725E-02
	0.260E-05	0	−0.746E-05	0.303E-04	−0.478E-04	−0.124E-03	−0.146E-02	−0.423E-02
1.56	0.442E-03	0.231E-02	0.116E-02	0.236E-01	0.993E-01	0.103	0.395	0.210
	−0.464E-04	−0.144E-04	−0.326E-04	−0.240E-03	−0.295E-03	−0.210E-03	−0.142E-02	−0.239E-02
	−0.320E-05	0.309E-04	−0.241E-05	−0.422E-04	−0.324E-03	−0.355E-03	−0.400E-02	−0.395E-02
1.23	0	0.235E-03	0.208E-02	0.182E-01	0.834E-01	0.124	0	0
	0	−0.216E-04	−0.177E-03	0.169E-04	0.110E-02	0.755E-03	0	0
	0	−0.786E-05	−0.753E-04	−0.322E-03	−0.702E-03	−0.282E-02	0	0

Table A2 Elements from the transfer function for $\cos\theta_0 = 0.5$.

r_e/g	0.198	0.266	0.356	0.477	0.640	0.858	1.150	1.542
25.00	0	0	0	0	0	0.383	0.541	0
	0	0	0	0	0	−0.816E-02	−0.891E-02	0
	0	0	0	0	0	0.528E-03	−0.768E-03	0
11.11	0	0	0	0	0.105	0.271	0.600	0
	0	0	0	0	−0.271E-02	−0.368E-02	−0.765E-02	0
	0	0	0	0	0.704E-03	0.128E-04	−0.176E-02	0
6.25	0	0	0	0.228E-01	0.115	0.230	0.631	0
	0	0	0	−0.641E-03	−0.173E-02	−0.196E-02	−0.559E-02	0
	0	0	0	0.327E-03	0.607E-03	−0.621E-03	−0.288E-02	0
4.00	0	0	0.845E-02	0.468E-01	0.811E-01	0.214	0.588	0
	0	0	−0.215E-03	−0.617E-03	−0.564E-03	−0.121E-02	−0.287E-02	0
	0	0	0.197E-03	0.444E-03	−0.272E-03	−0.106E-02	−0.352E-02	0
2.78	0	0.610E-02	0.254E-01	0.417E-01	0.761E-01	0.214	0.410	0
	0	−0.146E-03	0.165E-04	−0.106E-03	−0.436E-03	−0.618E-03	−0.170E-03	0
	0	0.192E-03	0.103E-03	−0.673E-04	−0.368E-03	−0.137E-02	−0.276E-02	0
2.04	0.834E-02	0.383E-02	0.113E-01	0.278E-01	0.757E-01	0.308	0.342E-01	0
	0.633E-04	−0.513E-04	−0.775E-04	−0.246E-03	−0.353E-03	0.114E-02	0.189E-03	0
	0.252E-03	0.149E-04	0.233E-04	−0.950E-04	−0.629E-03	−0.215E-02	−0.232E-03	0
1.56	0.164E-02	0.418E-02	0.980E-02	0.276E-01	0.110	0.186E-01	0	0
	−0.130E-04	−0.714E-04	−0.156E-03	−0.163E-03	0.119E-02	0.264E-04	0	0
	0.225E-04	0.185E-04	−0.797E-04	−0.437E-03	−0.115E-02	−0.341E-04	0	0
1.23	0.183E-02	0.404E-02	0.928E-02	0	0	0	0	0
	−0.493E-04	0.766E-05	0.286E-03	0	0	0	0	0
	−0.470E-04	−0.148E-03	−0.178E-03	0	0	0	0	0

Table A3. Elements from the transfer function for $\cos\theta_0 = 0.96$.

r_e/g	0.198	0.266	0.356	0.477	0.640	0.858	1.150	1.542
25.00	0	0	0	0	0	1.98	0.315	0
	0	0	0	0	0	−0.127E-02	−0.404E-05	0
	0	0	0	0	0	0.524E-05	−0.632E-04	0
11.11	0	0	0	0	0.192E-03	1.73	0.132E-01	0
	0	0	0	0	−0.118E-05	−0.726E-03	0.309E-05	0
	0	0	0	0	0.687E-06	−0.147E-03	−0.245E-05	0
6.25	0	0	0	0	0.377	0.824	0	0
	0	0	0	0	−0.738E-03	0.503E-03	0	0
	0	0	0	0	0.635E-03	−0.868E-03	0	0
4.00	0	0	0	0.334E-01	0.622	0.518E-01	0	0
	0	0	0	−0.137E-03	0.676E-04	0.945E-04	0	0
	0	0	0	0.290E-03	−0.537E-03	−0.130E-03	0	0
2.78	0	0	0.988E-02	0.239	0.850E-01	0	0	0
	0	0	−0.224E-04	−0.710E-04	0.223E-03	0	0	0
	0	0	0.148E-03	−0.986E-04	−0.475E-03	0	0	0
2.04	0	0.126E-01	0.810E-01	0.225E-01	0	0	0	0
	0	0.213E-04	−0.972E-04	0.124E-03	0	0	0	0
	0	0.212E-03	−0.205E-03	−0.251E-03	0	0	0	0
1.56	0.124-01	0.118E-01	0.161E-03	0	0	0	0	0
	0.329E-04	0.179E-04	0.354E-05	0	0	0	0	0
	0.362E-04	−0.194E-03	−0.299E-05	0	0	0	0	0
1.23	0	0	0	0	0	0	0	0
	0	0	0	0	0	0	0	0
	0	0	0	0	0	0	0	0